Research Article Vol. 33, No. 13 / 30 Jun 2025 / Optics Express 28898
Optics EXPRESS

Programmable meta-fluid antenna for spatial multiplexing in fast fluctuating radio channels

BAIYANG LIU,[1,2] KIN-FAI TONG,[3,4,6] KAI-KIT WONG,[4,5] CHAN-BYOUNG CHAE,[5] AND HANG WONG[2,7]

[1]College of Big Data and Internet, Shenzhen Technology University, Shenzhen, 518118, China
[2]State Key Laboratory of Terahertz and Millimeter Waves, Department of Electrical Engineering, City University of Hong Kong, Hong Kong SAR, China
[3]School of Science and Technology, Hong Kong Metropolitan University, Hong Kong SAR, China
[4]Department of Electronic and Electrical Engineering, University College London, London, WC1E7JE, UK
[5]Yonsei Frontier Lab, Yonsei University, Republic of Korea
[6]ktong@hkmu.edu.hk
[7]hang.wong@cityu.edu.hk

Abstract: Interference and scattering in fast-fluctuating radio waves, often considered undesirable, are inevitable in wireless communications, particularly in current mobile networks and the anticipated sixth generation (6G) systems, which are evolving into ultra-dense deployments. Current approaches relying on multiple-input multiple-output (MIMO) combined with artificial intelligence (AI)-aided signal processing suffer from drawbacks such as high power consumption and the need for wide bandwidth, raising scalability concerns. In this article, we present a radical approach that leverages the channel fading phenomenon to our advantage. Specifically, we propose what we believe to be a novel meta-fluid antenna architecture, referred to as the 'fluid' antenna system (FAS), which can exploit radio wave fluctuations with fine spatial resolution to opportunistically avoid interference, eliminating the need for complex signal processing. Our experimental results demonstrate that, under rich scattering conditions, the proposed meta-fluid architecture can harness the natural variations in radio waves to achieve spatial multiplexing. These breakthrough results demonstrate that scattering can be beneficial rather than harmful, and interference can be avoided rather than suppressed, fundamentally changing our perception of fading and our understanding of how interference should be managed in wireless communication networks.

1. Introduction

Although the fifth-generation (5G) mobile systems have been painted to be a revolutionary technology, they have yet to impress average smartphone users. The compelling use cases—namely, holographic communications [1,2] and tactile Internet [3,4]—prominently featured in 5G promotions are currently unavailable. This is because promotional events often dedicate specific spectral and energy resources to enable these use cases; however, in reality, resources are limited, and the mass provision of such demanding services is currently infeasible with existing technologies. This has prompted communication practitioners, researchers, and scientists to consider the improvements needed for the next generation, a.k.a. sixth-generation (6G) [5–7]. Among other ambitious key performance indicators (KPIs), one standout target is to hit more than 1000 bps/Hz spectral efficiency in 6G [8]. This target would mean that the communication link needs to operate at an extraordinary SNR of 3000 dB if a single-user point-to-point system is considered. A more realistic interpretation of the target is to require the network to share the spectrum among a large number of users while maintaining acceptable performance for each.

Multiple access techniques [9,10] govern how users are given access to the available spectral resources for communications. Traditional approaches rely on time-division multiple-access

#567923 https://doi.org/10.1364/OE.567923
Journal © 2025 Received 15 May 2025; revised 10 Jun 2025; accepted 11 Jun 2025; published 27 Jun 2025

Optics EXPRESS

(TDMA) and frequency-division multiple-access (FDMA) where users are provided with orthogonal, non-overlapped channels for communications because of their simplicity in interference management. Reconfigurable intelligent surfaces (RIS) and metasurfaces enhance channel capacity by shaping the wireless environment [11,12]. OAM and polarization multiplexing further increase spectral efficiency by enabling multiple data streams [13–15]. However, as mobile networks attempt to catch up with the rising demands under limited spectrum, it is increasingly necessary to share the same time-frequency channel over multiple communications. In doing so, proper interference management needs to be in place to ensure reliable communications. In 5G New Radio (NR), this is being achieved by the massive multiuser multiple-input multiple-output (MU-MIMO) technology [16].

The principle of MU-MIMO is simple. Assuming the availability of the channel state information (CSI) of the users, a multi-antenna base station (BS) can utilize signal processing to mix the signals cleverly from its antennas before transmitting to the users—a method called MU-MIMO precoding.

Unfortunately, the experience of massive MU-MIMO in 5G-NR has been somewhat underwhelming, raising doubts about the potential of extra-large MIMO (XL-MIMO) for 6G [17]. The main challenge is scalability, particularly the difficulty in upscaling the CSI acquisition process with many users and the complexity of computing the precoding solution. Reliable CSI acquisition is crucial for effective MU-MIMO precoding, but wireless channels change rapidly, making it harder to maintain CSI accuracy with more users. It is also worth mentioning two emerging multiple access techniques, non-orthogonal multiple access (NOMA) [18] and rate-splitting multiple access (RSMA) [19], which propose overlapping users on the same physical channel using advanced coding and decoding schemes. While NOMA was seriously considered during the 5G development cycle [20], RSMA is now entering 3GPP discussions for beyond 5G and 6G standardization. However, both NOMA and RSMA face challenges with CSI feedback and high decoding complexity, limiting their potential as massive spectrum-sharing solutions. A fundamentally different approach is needed to complement existing and emerging MU-MIMO technologies.

With the rapid growth of artificial intelligence (AI), some might feel optimistic about addressing the scalability issue in MU-MIMO [21]. As a matter of fact, deep learning has already been utilized to reduce the CSI feedback for massive MIMO systems in 5G [22]. Deep learning is also anticipated to be applicable to a wide range of design problems in the physical layer of 6G [23]. With that being said, however, the system performance is fundamentally dictated by the physical signals at hand, and AI will be powerless to change that. In light of this, the objective of this work is to break the physical boundaries of existing communication systems and explore opportunities to innovate multiple access technologies for wireless communications that scales well with the number of users.

In order to rethink multiple access, the concept of a new form of reconfigurable antennas, referred to as 'fluid' antenna system (FAS), which has recently been introduced to become an enabling technology for 6G [24,25], is highly appealing. FAS represents any software-controllable shape-flexible position-flexible antenna system for wireless communications. FAS is first of its kind in the wider area of reconfigurable antennas. From the information-theoretic perspective, FAS can be viewed as some new degree-of-freedom in the physical layer for enhancing communication performance. A recent tutorial article [26] provides a comprehensive coverage on many topics on FAS. Remarkably, through position reconfigurability, FAS gives a transceiver the ability to access the received signals in fine space. In contrast to having only one received signal at a *point* in space from a conventional fixed-position antenna, FAS makes it possible to receive signals from a prescribed *spatial region* with fine resolution. This change is fundamental because this expands the dimensionality of the received signals without necessarily increasing the number of radio-frequency (RF) chains accordingly. Importantly, this capability

Optics EXPRESS

enables access to the ups and downs of the wireless channel in space, which can be exploited for multiple access. In particular, a wireless channel, usually modelled as a complex coefficient characterizing both magnitude attenuation and phase shift, sums up the overall effect of radio wave propagation in a wireless environment and this can also be interpreted as the superposition of multiple propagation paths between the transmitter and receiver over a wireless link. A classical phenomenon is that a wireless channel imposes random attenuation and phase shift and the channel can disappear when the multiple paths happen to cancel each other, which is referred to as *fading*. This channel fading coefficient changes if the position of reception is different, as different propagation paths mix differently. Now, this is where FAS can be uniquely effective. Specifically, FAS is able to observe how the wireless channel varies over a given spatial region with fine resolution, and the fading phenomenon means that the FAS will likely see that at some positions, the channel disappears. In multiuser scenarios, FAS therefore can choose to activate the position where the channel of the aggregate interference disappears (or becomes very weak) and this is the fluid antenna multiple access (FAMA) concept proposed in [27]. The exciting result here is that interference avoidance is achieved without the need of CSI at the BS as in MU-MIMO precoding nor advanced coding and decoding as in NOMA and RSMA. Our interpretation of FAMA is to utilize the radio wave fluctuation and exploit the naturally created opportunity for spatial multiplexing.

The concept of FAMA was introduced by Wong *et al.* in 2022 [27,28] while subsequent efforts further looked to address its challenges in signal processing [29] and combine this with other technologies [30]. Nevertheless, existing results are largely limited to theoretical studies, and how FAMA can be realized in practice is not well understood. To implement a FAS, a straightforward approach is to employ liquid antennas, due to its shape flexibility [31–33]. Recently in [34], liquid-metal antennas were adopted to design a position-flexible FAS and the measurement data obtained were also used to test the feasibility of FAMA. Despite the positive results, the major criticism of the liquid-based approach is the slow response time in changing the position of FAS. The required response time is in the millisecond range or less (i.e., the channel coherence time) but changing the position of a liquid-based radiating object takes a little less than a second in the best case. A promising alternative is to use reconfigurable pixels to realize FAS [35]. In this approach, a reconfigurable radiating surface is composed of a matrix of tiny pixels, with the connections between pixels being optimized to reconfigure the radiation characteristics. This approach has recently been explored to implement FAS in [36], producing encouraging results. However, the results in [36] are still in a very early stage and there is lack of understanding of how the optimized connections between pixels link to the specific features in radiation. Also, whether the FAS in [36] is effective for FAMA is yet to be seen. There are also the ideas of coding on metasurfaces [37–44], leaky-wave antennas [45–48], pixel-based antenna [36] and moveable antenna [49] that are applicable to the design of FAS even though there have been no attempts except [36] so far to utilize these techniques to realize the concept of FAS. Presumably, it is possible to use positive-intrinsic-negative (PIN) diodes to control the operating state of each metasurface element, and the theory of leaky-wave antennas can be useful to design substrate integrated waveguides (SIWs) that manage the propagation of radio waves.

In this work, we take a radical approach that views scattering as a desirable factor that provides opportunity by nature to harness interference, as opposed to negating scattering by heavy signal processing to restore channel stability. This is achieved by a new form of reconfigurable antenna, referred to as meta-fluid antenna by integrating a slot-array antenna with coding-on-metasurface technique, to exploit the fine resolution in space to utilize the interference null naturally created due to scattering. The proposed idea is enabled by the fully electronically programmable meta-fluid architecture. Here we present the first demonstration of FAMA and show the potential application scenarios, which incorporates artificial massive-rich scattering transmitters and a meta-fluid antenna (see Fig. 1). We have successfully harnessed the power of electromagnetic

Optics EXPRESS

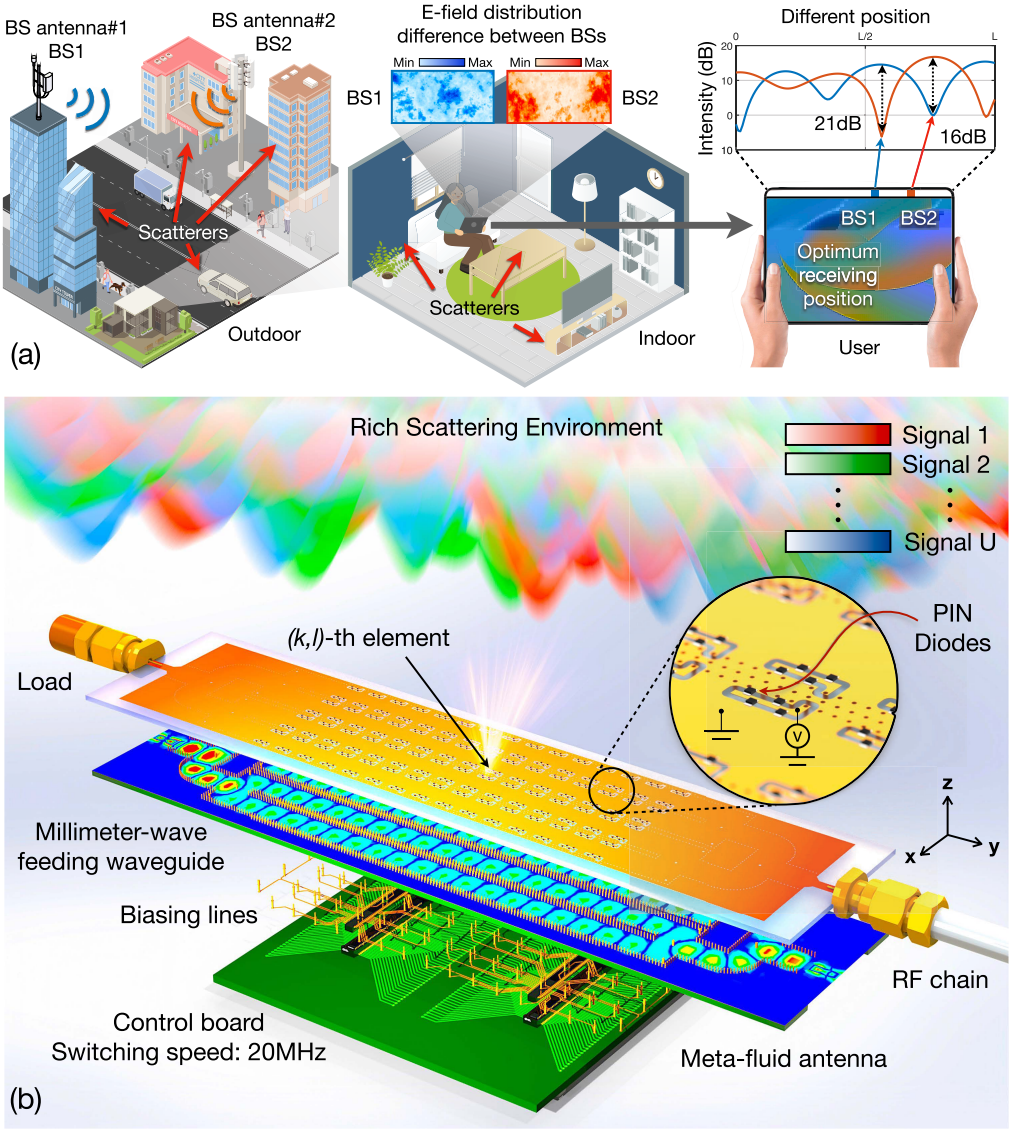

Fig. 1. Illustration of the concept of FAS and FAMA. (a) A downlink communication system is shown, where two distributed BSs are responsible for transmitting data to two mobile users in a typical rich-scattering environment (both outdoor and indoor). The figure in the middle also shows a user with a FAS mounted on her laptop, enabling the observation of the E-field distributions of the signals arriving from the two respective BSs. The figure on the right then illustrates the concept of FAMA. Specifically, this figure focuses on a particular horizontal dimension of the FAS and displays how the intensity of the radio signals changes along this dimension. It is clear that the radio signal intensity fluctuates, which gives rise to the opportunity for the FAS to avoid interference. (b) A layered illustration of the proposed 2D meta-fluid antenna architecture which uses PIN diodes to control the state of each meta-atom for activation/deactivation, and adopts a millimeter-wave SIW to gather the energy from the metasurface for radiation. The control of the meta-atom or radiating elements is managed by an FPGA underneath.

Optics EXPRESS

(EM) wave dynamics in space and time by strategically activating the elements of the metasurface to the position in which the SINR is maximized for multiple access, preventing the need for expensive signal processing at the BS side. This new approach has far-reaching implications for a broad range of wireless applications, sensing networks and encryption technologies.

2. Results

2.1. Principles of FAMA

Consider a wireless communication network where U users are being served on a shared physical channel by a BS in the downlink. The BS has U fixed-position antennas, with each antenna dedicated to transmit communication signals to one of the users. The assignment of BS antenna to user is unimportant in this work but can be easily done when needed in practice. At the user side, each user is equipped with a meta-fluid antenna system (FAS) that has the ability to switch to a 'good' radiating position in accordance with the fast-changing wireless channel conditions. The FAS at each user is assumed to have N preset positional points, arranged in a two-dimensional (2D) grid of I rows and J columns over a given surface; hence $N = I \times J$. All of these selectable positions share a common RF chain. Under this model, the received signal at the (i,j)-th position of FAS for user u can be expressed as (see Supplement 1, Supplementary Note 1 for the FAMA network model)

$$r_{i,j}^{(u)} = s_u g_{i,j}^{(u,u)} + \sum_{\substack{\tilde{u}=1 \\ \tilde{u}\neq u}}^{U} s_{\tilde{u}} g_{i,j}^{(\tilde{u},u)} + \eta_{i,j}^{(u)}, \tag{1}$$

where $u \in \{1,2,\ldots,U\}$, $i \in \{1,2,\ldots,I\}$, $j \in \{1,2,\ldots,J\}$ and s_u represents the transmitted symbol intended for user u, while $\eta_{i,j}^{(u)}$ denotes the zero-mean complex additive white Gaussian noise (AWGN) at the (i,j)-th position of the user. The term $g_{i,j}^{(\tilde{u},u)}$ describes the fading channel from the $\tilde{u}$-th BS antenna to the (i,j)-th position of user u. When $\tilde{u} \neq u$, this corresponds to the interfering channel while the $\tilde{u} = u$ case gives the desired channel. We will focus on the timescale where the fading channels are regarded as static to ease our discussion without loss of generality. In practice, channels do change however but the same process can be repeated every time changes happen.

In FAMA, user u switches its FAS to the position that maximizes the SINR, or signal-to-interference ratio (SIR) when noise is negligible at high SNR [27]. That is, the optimal position $(i^*,j^*)|_u$ is selected by

$$(i^*,j^*)|_u = \arg\max_{i,j} \frac{\mathbb{E}\left[\left|g_{i,j}^{(u,u)} s_u\right|^2\right]}{\mathbb{E}\left[\left|\sum_{\substack{\tilde{u}=1 \\ \tilde{u}\neq u}}^{U} g_{i,j}^{(\tilde{u},u)} s_{\tilde{u}} + \eta_{i,j}^{(u)}\right|^2\right]} \approx \arg\max_{i,j} \frac{\left|g_{i,j}^{(u,u)}\right|^2}{\sum_{\substack{\tilde{u}=1 \\ \tilde{u}\neq u}}^{U} \left|g_{i,j}^{(\tilde{u},u)}\right|^2}, \tag{2}$$

in which $\mathbb{E}[\cdot]$ returns the expectation of an input random entity. The theoretical performance in terms of outage probability for FAMA has been studied in [50,51], revealing promising results in multiple access.

What is missing in the literature is the experimental validation of the effectiveness of FAMA. This does not only require the highly reconfigurable FAS hardware to be designed and fabricated but also the experiments that give measurement data to validate the performance in real environments. This is the goal of this paper.

Optics EXPRESS

2.2. Meta-fluid antenna

Our proposed meta-fluid antenna consists of a 2D slot-array of $N = 120$ elements, arranged in $I = 8$ rows and $J = 15$ columns. The elements can be dynamically switched between radiating and non-radiating states, as illustrated in Fig. 2(a). This architecture effectively integrates 120 individual positions within a single RF chain. By utilizing a field-programmable gate array (FPGA) controller, a single element with 4 PIN diodes can be selectively activated to radiate energy from the waveguide to air, while the remaining elements remain in a non-radiating state. This enables the realization of a meta-fluid, with the interpretation that a genie is riding on the radio waves on the metasurface and able to dynamically activate a particular position for reception.

Technically speaking, a meta-atom is made up of two elements, referred to as the slot '+' and slot '−' elements, respectively, see Fig. 2(b). An important distinction between a meta-atom and a selectable position is that each meta-atom includes two selectable positions, one for each slot. Each element functions as a waveguide-fed magnetic dipole, extracting energy from the waveguide and emitting EM waves into the surrounding space. Given that the lattice size of the meta-atom is much smaller than the wavelength, the elements can be considered as sampling points that capture the energy of the guided waves propagating within the waveguide at their respective positions (see Supplement 1 for design details of the meta-atom). The magnetic field produced by the (k, ℓ)-th meta-atom in the far-field region at distance $d_{k,\ell}$ is written as

$$H_{k,\ell}(\theta) = -\frac{\pi f_0^2 m_{k,\ell} \cos\theta}{d_{k,\ell}} e^{-jk_0 d_{k,\ell} \sin\theta}, \tag{3}$$

where f_0 is the carrier frequency, θ is the observation angle relative to the meta-fluid antenna, k_0 is the propagation constant in free space, and $m_{k,\ell}$ is the polarized magnetic dipole moment at time t excited by the meta-atom as

$$m_{k,\ell} = P_{k,\ell} H_{k,\ell} = P_{k,\ell} H_0 e^{-j\xi_{\mathrm{gw}} x_{k,\ell}} e^{j2\pi f_0 t}, \tag{4}$$

where $P_{k,\ell}$ denotes the complex magnetic polarizability at the (k, ℓ)-th position, and $H_{k,\ell}$ signifies the instantaneous magnetic field produced at the (k, ℓ)-th position within the waveguide structure. Additionally, H_0 is the corresponding magnitude of the magnetic field, $x_{k,\ell}$ denotes the corresponding propagation distance in the waveguide, and ξ_{gw} is the propagation constant for a guided wave, given by

$$\xi_{\mathrm{gw}} = \sqrt{\omega^2 \mu\varepsilon - \left(\frac{\pi}{W_{\mathrm{eff}}}\right)^2}, \tag{5}$$

where μ and ε are the permeability and permittivity of the medium, ω is the carrier angular frequency, and W_{eff} denotes the effective width of the waveguide.

Noting that the magnetic current within the waveguide exhibits a phase reversal between the upper and lower slots, for ease of reference, we refer to them as the slot '+' and the slot '−', respectively. For differentiation between the two slots along the longitudinal axis of the waveguide, the magnetic polarizability and distance to the far-field observation point for the upper slot are denoted as $P^+_{k,\ell}$ and $d^+_{k,\ell}$, respectively, while those for the lower slot are $P^-_{k,\ell}$ and $d^-_{k,\ell}$. The slots in each meta-atom are controlled by PIN diodes. Different states of the slots will result in different radiation amplitudes and phase adjustments, which are summarized as follows:

$$\begin{aligned} P^+_{k,\ell} &= \begin{cases} P_0 e^{-j0} & \text{for state ON}^+, \\ 0 & \text{for state OFF}^+, \end{cases} \\ P^-_{k,\ell} &= \begin{cases} P_0 e^{-j\pi} & \text{for state ON}^-, \\ 0 & \text{for state OFF}^-. \end{cases} \end{aligned} \tag{6}$$

Optics EXPRESS

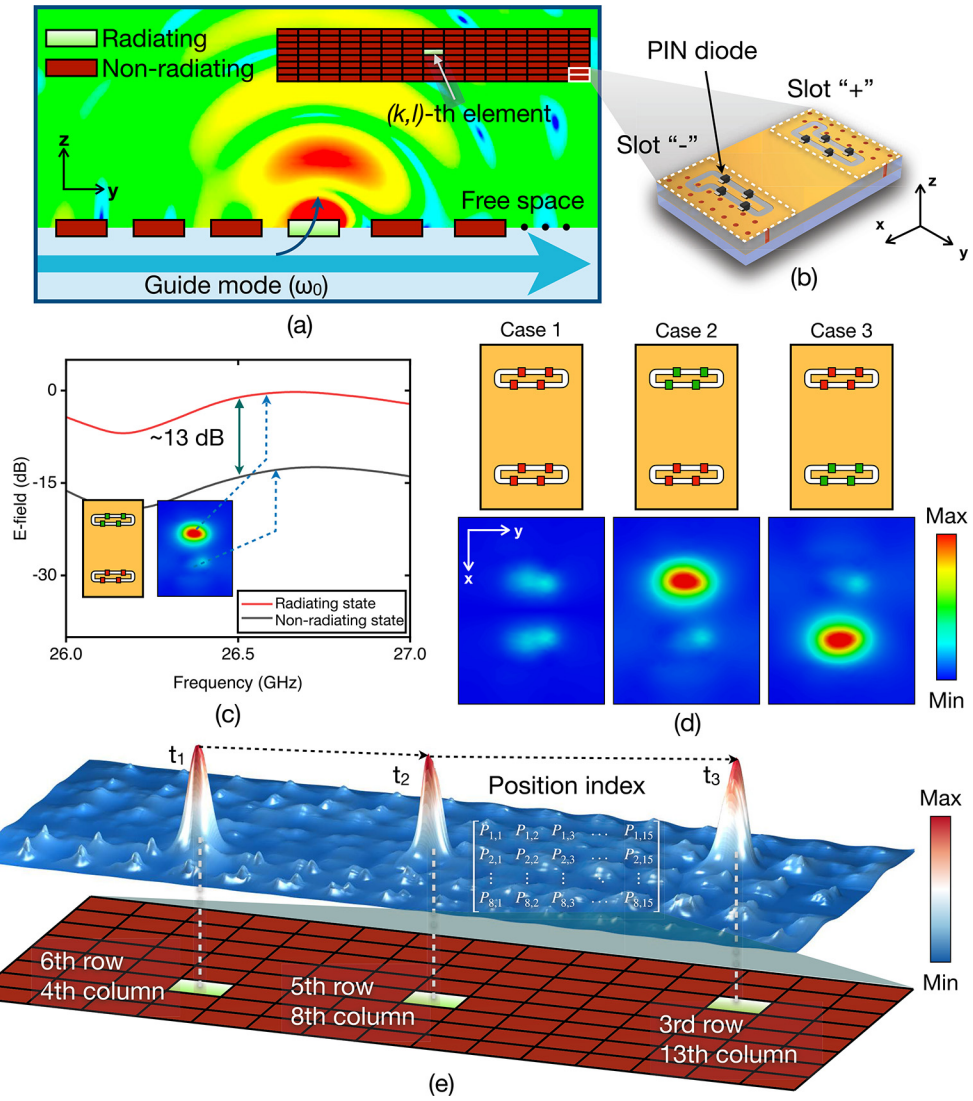

Fig. 2. The working principle of the proposed meta-fluid antenna. (a) This shows a schematic representation of the meta-fluid antenna architecture with 8×15 radiating elements and the simulated radiating pattern in the *yz*-plane if a given element is activated. (b) This figure shows the basic 3-dimensional (3D) structure of a meta-atom which consists of an upper element and a lower element. Each element is connected and controlled by 4 PIN diodes. (c) This figure illustrates the simulated E-field results against frequency focusing on one meta-atom if the upper element is in an 'ON' state but the lower element is in an 'OFF' state. The results show an approximate 13 dB difference in their E-fields between the two elements. (d) The figures display the E-field distributions in the *xy*-plane in the three possible states for the meta-atom. (e) This figure depicts the distribution of E-fields on the surface of the proposed meta-fluid antenna at different time instances when a different element is activated. The E-field distribution resembles a rippling noise and interference floor, with a spike wave appearing at an activated element.

Relevant to the functionality of position-flexible FAS, three states of a meta-atom are of interest: (1) $\text{OFF}^{+}\&\text{OFF}^{-}$; (2) $\text{ON}^{+}\&\text{OFF}^{-}$ and (3) $\text{OFF}^{+}\&\text{ON}^{-}$. This corresponds to the cases that

Optics EXPRESS

both of the slots are off (Case 1) or either one of the slots is on (Case 2 & Case 3), respectively, as depicted in Fig. 2(d). For each of the 'ON' state, its magnetic field can be computed by substituting Eq. (4) and Eq. (6) into Eq. (3). As such, the far-field expression for the (k,ℓ)-th meta-atom in the 'ON' state can be expressed as

$$H_{k,\ell}(\theta) = \begin{cases} -\left(\pi H_0 f_0^2 \cos\theta\right) e^{j2\pi f_0 t} \left[\frac{P^+_{k,\ell}}{d^+_{k,\ell}} e^{-j\left(\xi_{\mathrm{gw}} x_{k,\ell} - k_0 d^+_{k,\ell} \sin\theta\right)}\right] & \text{for state ON}^+\&\text{OFF}^-, \\ -\left(\pi H_0 f_0^2 \cos\theta\right) e^{j2\pi f_0 t} \left[\frac{P^-_{k,\ell}}{d^-_{k,\ell}} e^{-j\left(\xi_{\mathrm{gw}} x_{k,\ell} - k_0 d^-_{k,\ell} \sin\theta\right)}\right] & \text{for state OFF}^+\&\text{ON}^-. \end{cases} \tag{7}$$

By switching the diodes between 'ON' and 'OFF' states, the radiation of the fields can be selectively blocked or allowed to pass through. A comparison of the electric field (E-field) differences between radiating and non-radiating states reveals a significant 13 dB difference, as seen in Fig. 2(c). In the meta-fluid antenna, the slot '+' and slot '−' will not be radiating at the same time, as their radiation will cancel from each other if both slots are in the 'ON' state. Furthermore, to showcase the fluidic E-fields, the surface fields on the meta-fluid antenna are illustrated with varying opening slots and at different time instances (see Supplement 1 for design details of the meta-fluid antenna). This demonstrates the fluctuation of EM waves over the metasurface, accessible by the proposed meta-fluidic architecture, as shown in Fig. 2(e).

2.3. Rich-scattering generators

To facilitate our experiments, we need to emulate the propagation conditions and characteristics of real environments in our laboratory setup. In particular, we design a waveguide-fed generator that radiates disordered beams, resulting in diverse, random E-field patterns to mimic what appears in real rich-scattering environments. Our generator is a waveguide surface that contains many randomly distributed slots. Figure 3(a) shows three different generators, each responsible for emulating the propagation environment from one particular user to the developed FAS receiver.

To accurately determine the total surface radiation, it is necessary to account for the far-field contributions from all the slots. In this scenario, the overall far-field radiation from the generator can be characterized as

$$\begin{aligned} H(\theta) = &-\left(\pi H_0 f_0^2 \cos\theta\right) e^{j2\pi f_0 t} \\ &\times \sum_{m=1}^{M_s} \sum_{n=1}^{N_s} \left[\frac{P^+_{m,n}}{d^+_{m,n}} e^{-j\left(\xi_{\mathrm{gw}} x_{m,n} - k_0 d^+_{m,n} \sin\theta\right)} + \frac{P^-_{m,n}}{d^-_{m,n}} e^{-j\left(\xi_{\mathrm{gw}} x_{m,n} - k_0 d^-_{m,n} \sin\theta\right)}\right], \end{aligned} \tag{8}$$

where $2M_s \times N_s$ denotes the total number of slots in the waveguide structure, and the rest of the variables/parameters are defined in a similar way as in the case of meta-fluid antenna earlier, except that we now have fixed slots but not meta-atoms. Also, there are M_s rows of slots and each row consists of an upper '+' row and a lower '−' row of slots. Note that in the meta-fluid antenna, the meta-atoms are tuneable but the slots here are not.

For the generator, the radiating units are discrete slots, and the input energy is radiated out through the slots. For this reason, we need to consider the radiation efficiency η of each radiating unit. For the slots, their radiation efficiency is related to the attenuation constant in y-direction, α_y (according to the geometry in Fig. 3(b)), and the offset distance Δl from the waveguide center, i.e.,

$$\eta = 1 - e^{-2\alpha_y \Delta l}. \tag{9}$$

Let us focus on a particular row (in the y-direction), i.e., any of the M_s rows, upper or lower, of each generator. It is possible to work out the radiation power resulting from a particular slot, say

Optics EXPRESS

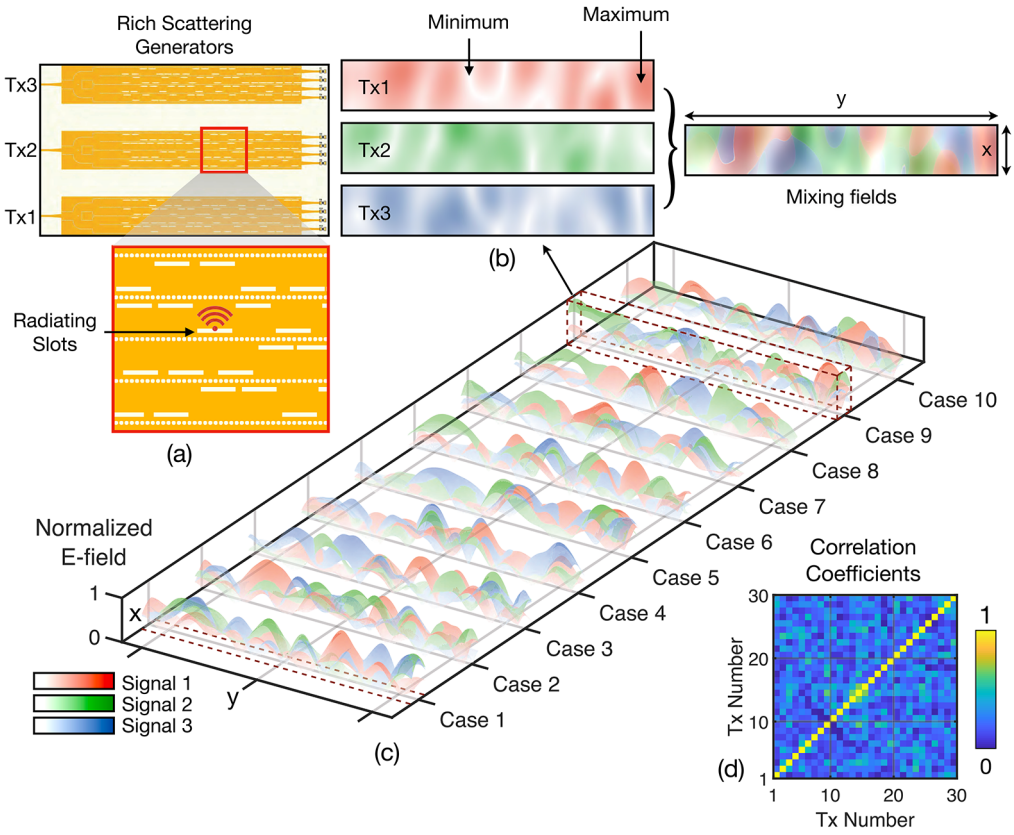

Fig. 3. Rich-scattering generators and their properties. (a) This shows the schematic of three rich-scattering generators with arbitrarily placed slots. A zoom-in picture highlights that each generator has several rows of slots and each row has an upper array and a lower array of randomly placed slots. A slot represents a position where radio wave is let out. Therefore, a generator outputs a mixture of radio waves out from the slots, mimicking the effect of scattering observed in real propagation environments with scatterers. (b) This figure shows the E-field distribution observable at different positions of the antenna prototype from each of the generators (LEFT), and that from all of the generators (RIGHT). (c) This figure illustrates all the E-field distributions observable at the meta-fluid antenna from all the generator-transmitters (Tx1, Tx2 and Tx3) in all 10 cases. (d) A numerical analysis of all 30 E-field data (3 transmitters and 10 independent situations) generated by the rich-scattering generators reveals their statistical independence, as demonstrated by the correlation coefficient matrix. This confirms that the fabricated generators can accurately emulate the characteristics of rich-scattering channels.

n_s, which can be found as

$$P_{n_s}^{\text{slot}} = \eta_{n_s} \prod_{n=1}^{n_s-1} (1-\eta_n)\, P_{\text{in}}, \tag{10}$$

where P_{in} denotes the input power and η_n can be obtained using Eq. (9). From Eq. (10), it is reasonable to see that the radiation power is stronger (or weaker) if it is closer to (or farther away from) the input. Now, if we take into account all the M_s rows in the waveguide-fed generator considering the use of a power divider to split the input power onto the M_s channels, then the

Optics EXPRESS

radiation power from the (m_s, n_s)-th slot can be easily obtained as [52]

$$P^{\text{slot}}_{m_s,n_s} = \eta_{m_s,n_s} \prod_{n=1}^{n_s-1} \left(1 - \eta_{m_s,n}\right) \frac{P_{\text{in}}}{M_s}, \tag{11}$$

where the respective variables are extended to cope with the 2D indices on the waveguide-fed generator. Finally, substituting (11) into (8) gives the overall far-field radiation

$$\begin{aligned} H(\theta) = &-\left(\pi H_0 f_0^2 \cos\theta\right) e^{j2\pi f_0 t} \frac{P_{\text{in}}}{M_s} \\ &\times \sum_{m=1}^{M_s} \sum_{n=1}^{N_s} \left[\frac{P^+_{m,n}}{d^+_{m,n}} e^{-j(\xi_{\text{gw}} x_{m,n} - k_0 d^+_{m,n} \sin\theta)} + \frac{P^-_{m,n}}{d^-_{m,n}} e^{-j(\xi_{\text{gw}} x_{m,n} - k_0 d^-_{m,n} \sin\theta)} \right] \\ &\times \eta_{m,n} \prod_{l=1}^{n-1} (1 - \eta_{m,l}) \,. \end{aligned} \tag{12}$$

To provide sufficient representation of real-world environments, we have made 30 such rich-scattering generators, all different with arbitrarily placed slots. We divide them into three groups and each group represents 10 independent wireless channel realizations from one transmitter. As a result, those generators are sufficient to test a 3-user FAMA system over 10 independent wireless environments. Our experiments will be discussed in the next section.

In Fig. 3(c), we illustrate the disordered fields transmitted through these rich scattering generators to the meta-fluid antenna receiver. It can be observed that different transmitters are making different radio waves emitting through the generators, mimicking the radio wave propagation phenomena over the metasurface of the meta-fluid antenna. To see that our generators produce radio waves that align with the theoretical rich-scattering model [53] and that these channels provide the conditions for FAMA to thrive, we use the measurement data from the generators and evaluate their correlation coefficients by

$$\rho(\mathbf{E}_i, \mathbf{E}_j) = \frac{\mathbf{E}_i \mathbf{E}_j^H}{\|\mathbf{E}_i\| \|\mathbf{E}_j\|}, \tag{13}$$

in which $\mathbf{E}_i$ for $i = 1, 2, \ldots, 30$ denotes the complex-valued row vectors for the E-field values received at all the switchable positions of the meta-fluid antenna receiver from the i-th generator, the superscript H is the hermitian operator, and $\|\cdot\|$ returns the norm of an input vector. Therefore, $\rho(\mathbf{E}_i, \mathbf{E}_j)$ measures how much the E-fields $\mathbf{E}_i$ and $\mathbf{E}_j$ are correlated. The results in Fig. 3(d) show that the correlation matrix looks like an identity matrix with the off-diagonal entries being quite small. This means that the E-fields arriving at a receiver from different transmitters are nearly independent, which provides the ideal condition for FAMA to dodge interference (see Supplement 1 for design details of the rich-scattering generators). Importantly, the method used to generate the environment does not affect the conclusion of this work. In fact, we find that our experimental setup yields results that more closely align with what are expected in Rayleigh fading environments. This method is therefore valid and offers robust validation of our experimental setup (see Supplement 1 Figure S6).

2.4. Experimental validation for FAMA

In this section, we present a prototype of the meta-fluid antenna and the experimental setup for demonstrating the feasibility of FAMA using the proposed meta-fluid antenna prototype, as shown in Figs. 4(a) and 4(b). Our experiments utilize the waveguide-fed generators to emulate the rich-scattering propagating characteristics seen in real-world environments. The fabricated

Optics EXPRESS

meta-fluid antenna is designed with a unique architecture that enables position switching, featuring $8 \times 15 = 120$ elements, i.e., 120 switchable positions. Each element can be independently controlled to switch between different operating states, allowing for dynamic reconfiguration of radiation position (or the resulting aperture) of the antenna. This is achieved through the use of PIN diodes, which are integrated into each element and controlled by an integrated control board. The control board is used for the operation of the meta-fluid antenna, as it connects to each PIN diode through biasing vias that provide the necessary DC current to switch the diodes between their 'ON' and 'OFF' states. Figures 4(c) and 4(d) show the front and back views of the meta-fluid antenna prototype, with the back view also showing brief details of the integrated control board. Besides, the meta-fluid antenna operates at a center frequency of 26.5 GHz with a bandwidth of 1 GHz.

Our 30 waveguide-fed generators represent 10 independent experiments (Case 1 to Case 10) for a 3-user FAMA system, with the meta-fluid antenna prototype as the receiver terminal (labelled as 'Rx'). During the experiments, the meta-fluid antenna was connected to one of the four ports of a vector network analyzer (VNA), serving as the receiving antenna, while the transmitter group, comprising three random E-field emitting antennas in the form of the 3-user waveguide-fed generators, was connected to the remaining three ports (labelled as 'Tx1', 'Tx2' and 'Tx3', respectively, see Fig. 4(b)). This setup enabled us to measure the received SINR of the meta-fluid antenna receiver with a varying activated position, thereby allowing us to understand the interference immunity of FAMA using the newly designed FAS. Specifically, any transmitter (Tx1, Tx2 or Tx3) can be viewed as the user of interest but if Tx1 is the user of interest, then Tx2 and Tx3 will be the interferers at the meta-fluid antenna receiver. In our experiments, we consider all the possible combinations so there is no bias towards a particular transmitter.

In Fig. 5, we provide the experimental results that illustrate the achievable SINR performance of FAMA using the meta-fluid antenna for a given channel realization (Case 5 of the generators). In Fig. 5(a), the situation considers Tx1 being the desired user and Tx2 and Tx3 being the interferers while Fig. 5(b) considers that Tx2 is the desired user and in Fig. 5(c), Tx3 is the desired user, with the other transmitters being the respective interferers. The results provided include the SINR data at the meta-fluid antenna (Rx) over the frequency range between 26 GHz and 27 GHz and at each frequency, the received SINRs of Rx with all the 120 possible activated positions are shown. The results clearly demonstrate that at any given frequency, the meta-fluid antenna obtains a large range of SINR values when its activated position changes, confirming the concept of FAMA via position-flexible FAS and that the benefits of FAMA are realizable by the proposed meta-fluid antenna prototype. In the figures, we have also marked the position of maximizing the SINR by FAMA at an arbitrary frequency point in all three situations, from Figs. 5(a) to 5(c). It is apparent that in all three situations, the meta-fluid antenna Rx can achieve a high SINR (>10.90 dB), meaning that the two interferers are satisfactorily avoided. Note that calculating the SINR of the proposed system can be accomplished by taking turn to activate the position of each meta-cell. With the high switching speed of 20 MHz, the SINR measurement at the FAS is easily achievable.

While the results in Fig. 5 are encouraging, they are focused on environment of Case 9. Figure 6 therefore provides the results of all the experimental environments (Case 1 to Case 10) to have a more complete understanding of the achievable performance of FAMA using the proposed meta-fluid antenna prototype. Additionally, we provide the SINR measurement data if the meta-fluid antenna Rx is replaced by a conventional fixed-position antenna for comparison. For clarity, we select the results at frequency 26.5 GHz but our general discussion is applicable to other operating frequencies permissible for the meta-fluid antenna. The results in Fig. 6 are given in three bar-charts, each representing a particular transmitter being the desired user of interest. Ten bars illustrate the ranges of SINR obtained by the meta-fluid antenna Rx for the ten independent experiments (Case 1 to Case 10). For any given case, the results indicate a good

Optics EXPRESS

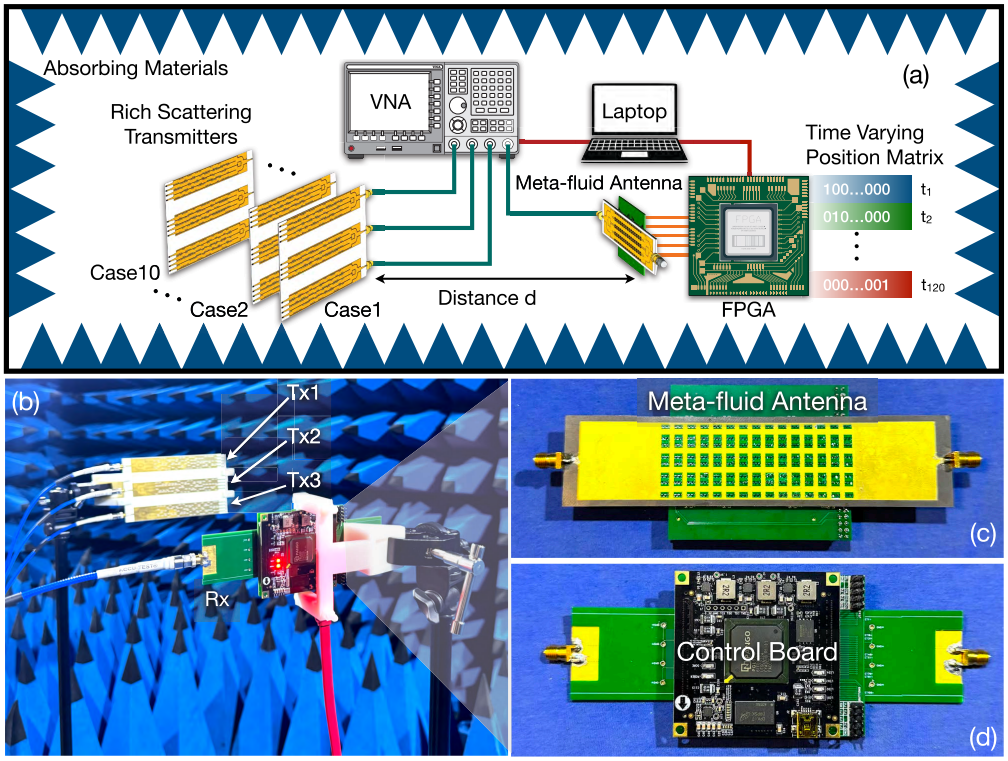

Fig. 4. The experimental setup of the FAMA system utilizing the meta-fluid antenna prototype Rx. (a) The schematic of the system setup is shown, which comprises the meta-fluid antenna as the receiver (Rx) and a rich-scattering generator group as the transmitters (Tx1, Tx2 and Tx3) with a communication distance of $d = 0.5$ meters. A rich-scattering generator group represents a particular situation of three transmissions undergoing independent scattering. Ten independent groups (or cases) are tested in the experiments. At the Rx, the SINR is measured using a VNA, while a laptop is used to input a time-varying position matrix, going through all 120 different positions, of the meta-fluid antenna. The laptop also controls the VNA to record the synchronizing channel data. (b) A photo shows the rich-scattering generators as the transmitter group and the meta-fluid antenna prototype in the chamber for measurement. Additionally, a red cable, which serves as the DC power cable for the FPGA, is also visible. The transmitter group and the receiver are separated by a distance of 0.5 meters. (c) This photo shows the front view of the antenna prototype with two ports, one connecting to a 50Ω load and another to the RF chain. The front side of the meta-fluid antenna is composed of 8 rows and 15 columns, totalling 120 elements. Each element is controlled by 4 PIN diodes, enabling toggling between the 'radiating' state and the 'non-radiating' state. (d) This photo shows the back view of the meta-fluid antenna attached to the integrated control board, which is seamlessly integrated with the antenna section through biasing vias. By reprogramming the FPGA, the radiating position of the meta-fluid antenna can be altered, allowing for dynamic control of the radiation pattern of the antenna.

range of SINR values, high and low, suggesting that the meta-fluid antenna experiences different levels of interference as the activated position changes–an essential feature for FAMA to work well. Evidently, in all the cases considered, the meta-fluid antenna Rx is able to achieve a decent SINR performance by simply changing the activated position. The worst case was Tx1 in Case 5 that obtained an SINR of 5.05 dB while the best case was Tx3 in Case 5 achieving an SINR of

Optics EXPRESS

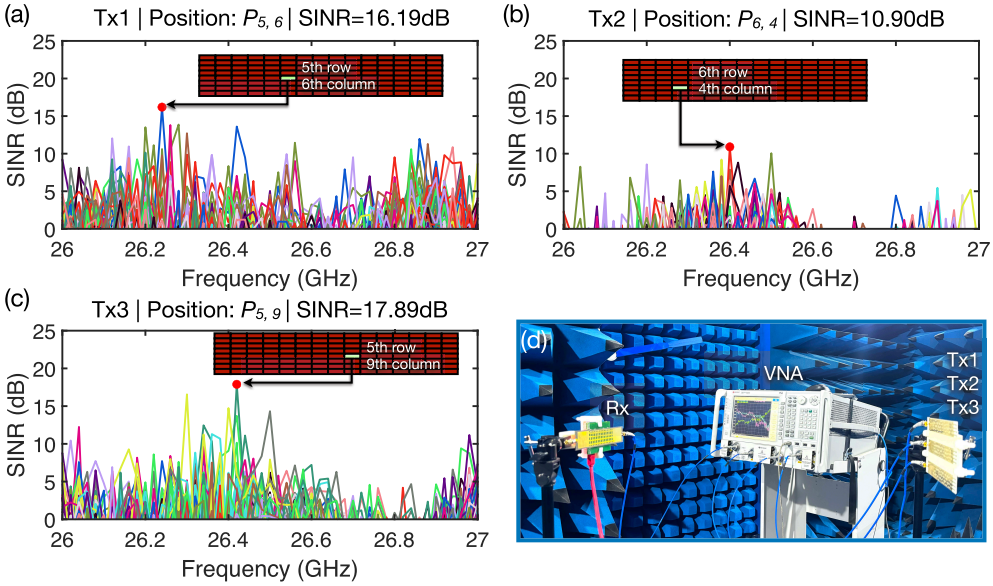

Fig. 5. The SINR measurements at the meta-fluid antenna prototype in the frequency range 26 to 27 GHz in Case 9 of the transmitter group. (a) This figure shows the measured SINRs against the frequency in the situation where Tx1 is considered as the desired user and Tx2 and Tx3 are the interferers. Moreover, at 26.25 GHz, the SINR at the $(5, 6)$-th position of the meta-fluid antenna is highlighted, which is the maximum SINR achievable by the meta-fluid antenna (16.19 dB). (b) Similar results are provided for the situation where Tx2 is the desired user and Tx1 and Tx3 are interferers. In this case, the maximum SINR at 26.4 GHz is highlighted, which corresponds to 10.90 dB at the $(6, 4)$-th position of the meta-fluid antenna. (c) Finally, the SINR results for the situation with Tx3 being the desired user and Tx1 and Tx2 being the interferers are shown. The $(5, 9)$-th position at a frequency near 26.43 GHz is highlighted, achieving an SINR of 17.89 dB. (d) A photo shows the complete setup connecting both the meta-fluid antenna and the transmitter group to a VNA for conducting the measurements.

14.33 dB. Figure 6(d) further uses Tx3 in Case 2 as an example to unpack all the SINR values achievable by the meta-fluid antenna Rx at all the 120 possible activated positions. Note that, the proposed spatial multiplexing technique can be applied for more users (see Supplement 1 of FAMA for more users). On the other hand, in order to highlight the unique performance that the meta-fluid antenna achieves, Fig. 6(e) provides the SINR results for both the meta-fluid antenna Rx and the conventional antenna Rx for comparison . For the results of the proposed meta-fluid antenna, only the maximum SINR values are shown, which corresponds to the FAMA performance. The number of reconfigurable elements influences the maximum achievable SINR. As the number of elements increases, providing a higher probability of finding a configuration that yields improved signal discrimination and higher SINR. Therefore, increasing the array aperture or element count enhances the system's ability to adaptively manage interference and optimize communication performance.

Moreover, a high-gain fixed-position horn antenna is used as the conventional antenna (see Supplement 1 for more information about the conventional fix-position antenna). All 10 cases or experiments are considered. The results reveal significant performance gains using the meta-fluid antenna Rx over the conventional antenna, and that the conventional antenna Rx fails to have any meaningful SINR in all the cases, indicating that the conventional Rx is overwhelmed by severe interference. Note that, for our concept verification, traditional antenna metrics such as radiation

Optics EXPRESS

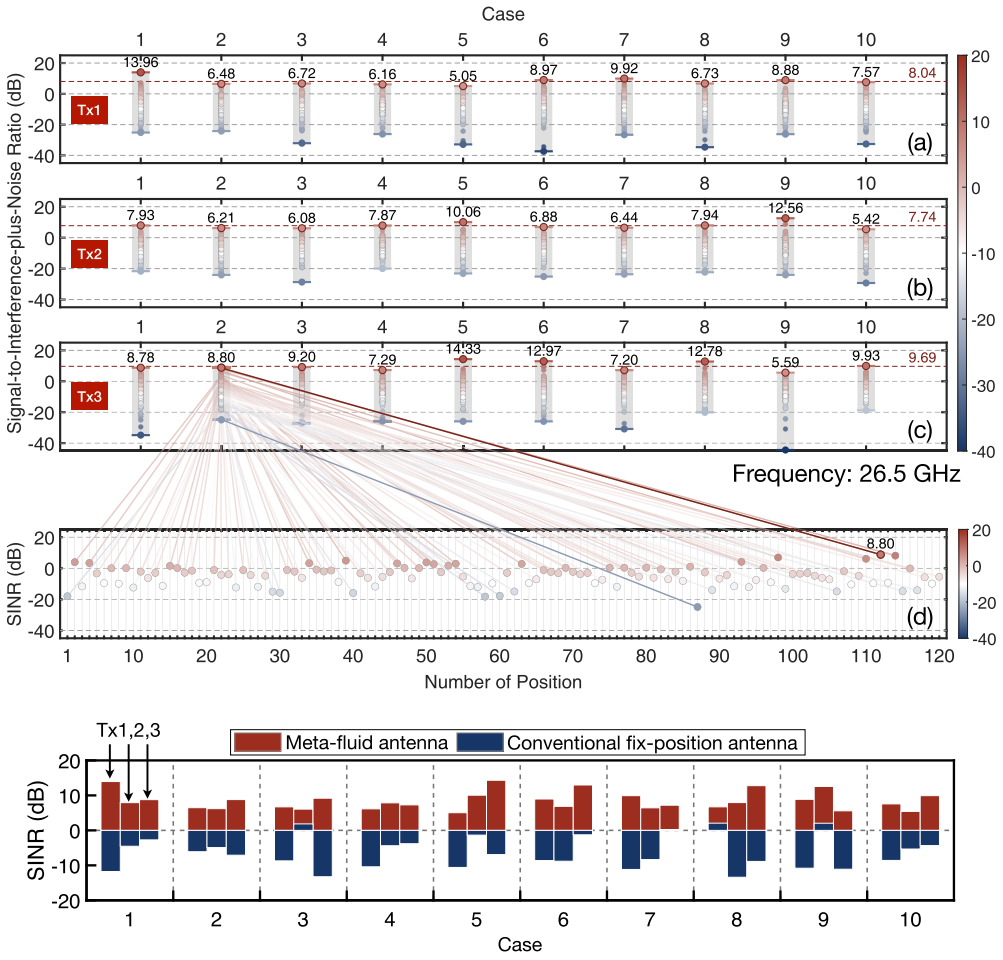

Fig. 6. The SINR measurement data at the meta-fluid antenna in all the propagation situations (Case 1 to Case 10) at 26.5 GHz. (a) This figure focuses on the situation where Tx1 is the desired user in the calculation of SINR. The ranges of the SINR observable at the meta-fluid antenna are shown in all 10 cases. In this situation, the average SINR over all the cases is also marked as 8.04 dB. (b) This figure provides similar SINR data but in the situation where Tx2 is considered as the desired user. In this situation, the average SINR achievable by the meta-fluid antenna is 7.74 dB. (c) This figure considers the situation treating Tx3 as the desired user and Tx1 and Tx2 as the interferers. In this case, the average SINR at the meta-fluid antenna is calculated to be 9.69 dB. (d) Additionally, we use Case 2 of Tx3 as an example to illustrate the actual received SINRs at all the possible 120 positions of the meta-fluid antenna. It can be seen that position number 112 at the meta-fluid antenna achieves the maximum SINR of 8.80 dB. (e) This figure provides the SINR performance comparison between the maximum SINR achievable by the meta-fluid antenna and the received SINR by a conventional fixed-position antenna.

pattern and S-parameters are not the focus. Instead, the objective is to confirm the ability of the proposed meta-fluid antenna to effectively avoid interference in an artificial Rayleigh fading environment. The experimental results are confirming the successful implementation of FAS and demonstration of the FAMA concept. The choice of a horn antenna was intentional and serves as an optimistic benchmark, as it allows for better interference management and a controlled

Optics EXPRESS

SINR. The unidirectional horn antenna, compared to an omnidirectional antenna, normally achieves a higher SINR due to its ability to suppress interference from unwanted directions. As such, it represents the upper bound of SINR performance for non-reconfigurable antennas. It is encouraging to see that the proposed meta-fluid antenna performs much better than this optimistic benchmark in terms of communication performance. This comparison further validates the capability of the meta-fluid antenna in rich-scattering environments.

3. Discussion

It is important to understand that the proposed meta-fluid antenna does not fall into the category of conventional reconfigurable antennas even though pin-diodes are used for reconfiguration. Conventional reconfigurable antennas are limited to changing a range of radiation characteristics (e.g., operating frequency, efficiency and so on) and are never designed to have the ability to reconfigure the position of the antenna aperture. The reason is that typical antenna experts do not see the benefits of it from purely the perspective of designing a functional antenna. However, wireless communications concerns more than just the radiation efficiency of an antenna and the exact position the signal is being received is uniquely important. Specifically, a key feature to wireless communications is that the received signal at any given position is randomly attenuated (according to Rayleigh fading under rich scattering), meaning that the communication performance varies according to the antenna position at any given time. This has led to the emerging concept of FAS which has been greatly impacting the wireless communication community [24–26] and motivates us to design for the first time an antenna that can reconfigure the position of its aperture to exploit the signal variation in the spatial domain. Our main contribution is the meta-fluid antenna architecture that can dynamically change the position of its radiation aperture over a 2D designated area by controlling the pin-diodes. This adaptability leverages the spatial diversity within a Rayleigh fading environment, allowing us to exploit channel variations for enhanced signal reception and mitigate interference. Moreover, this work represents the first experimental validation of the FAMA concept achieved through a new form of reconfigurable antenna, referred to as FAS, a contribution we believe is unprecedented in existing literature.

Contrasting to MIMO in which its spatial diversity is dictated by the number of RF chains at the mobile side, FAS unleashes a totally new degree of freedom through position reconfigurability in the spatial domain even when the number of RF chains is fixed. Specific to multiuser communications on the same physical channel, FAS recognizes the classical fading phenomenon that signal magnitude fades differently at different locations depending upon how multiple propagation paths combine, and uses it to our advantage for avoiding interference at the receiver end by adapting the antenna position. This fundamentally changes the way in which interference is mitigated in wireless networks. Conventionally, this is done by complex signal processing (called precoding) at the BS side which requires the availability of CSI of all users involved. The FAS approach referred to as FAMA, however, eliminates the need of CSI estimation and feedback to the transmitter as well as the complex optimization of precoding, and deals with interference as they arrive at the receiver. Therefore, there is great potential of FAMA to improve the scalability of multiuser wireless communications. While theoretical results reporting the amazing performance of FAMA have emerged in recent years and it is always desirable to consider a wide range of performance metrics for a more complete evaluation, experimental results are absent and there is also no known prototype successfully designed for FAS and for validation of FAMA. This work is therefore original and significant in that this serves as the first-ever FAS antenna design realizing the concept of position reconfigurability, and tested experimentally for FAMA.

Finally, it is worth mentioning that CSI estimation for FAS has been addressed in [54] and machine learning techniques have also been shown to find many applications on different FAS

Optics EXPRESS

communication problems, e.g., [29,30,55–60]. For more discussion, readers are referred to [26]. In future work, it would be important to extend the experimental setup to include real propagation environments. While our current setup, using artificial rich-scattering generators, effectively emulates Rayleigh fading conditions, testing in real environments will provide stronger evidence of FAS capabilities and the robustness of FAMA in realistic scenarios.

4. Conclusion

While the proposition of mitigating interference by antenna position reconfigurability following the emerging concept of FAS is exciting and numerous theoretical work has already reported its extraordinary performance to wireless communications, experimental validation is lacking and the effectiveness of FAS remains a hopeful speculation. To fill this gap, this paper has made two key contributions. First, by leveraging programmable waveguide feeding, we designed and fabricated a software-controlled meta-fluid antenna that can reconfigure the position of radiation on demand over a given surface, achieving the functionality of a position-flexible FAS for the first time. This is the unique feature of FAS which eliminates the need of expensive signal processing at the transmitter side, a major obstacle in the state-of-art precoding scheme used in 5G. The second major contribution of this paper is to provide experimental validation of using FAS for multiuser communications on a shared channel, referred to as FAMA in the communication community. Specifically, we fabricated multiple waveguide-fed generators with arbitrarily placed slots to emulate real-world radio propagation environments with rich scattering. The idea of FAMA was put to test using the prototype as the receiver terminal in a 3-user scenario (one desired transmitter and two interferers). Our experiments validated that FAMA is feasible using the proposed meta-fluid antenna and an average of more than 15 dB received SINR is obtained over all the cases considered. When the number of users increase, the SINR performance tends to degrade due to higher interference. However, this can be compensated by increasing the number of transmitter states, which enhances spatial diversity and improves the system's ability to separate user signals effectively. Overall, our findings provided solid experimental evidence that FAMA is practically achievable and obtains promising performance that paves the way for scalable multiple access technologies. Last but not least, the results demonstrated the superiority of the proposed meta-fluid antenna over a conventional fixed-position antenna, reaffirming the importance of FAS.

5. Materials and methods

All simulations in this study were conducted using CST Microwave Studio 2024. PIN diodes (MADP-000907-14020) were implemented on the meta-fluid antenna and modeled as an equivalent series circuit. For the 'OFF' state, which activates the radiating slot, the diodes were characterized by $C = 0.025$ pF and $L = 30$ pH. In the 'ON' state, which blocks the remaining slots, the diodes exhibited $R = 7.8\ \Omega$ and $L = 30$ pH. E-field correlation coefficients and SINR calculations were performed using Matlab 2023. The meta-fluid antenna and rich-scattering generators were fabricated using the printed circuit board (PCB) technology. The AVP50G FPGA core board was implemented on the meta-fluid antenna, allowing control of its 120 IO ports through Verilog HDL programming. The output signals could switch at frequencies up to 1 MHz, and the switching frequency of PIN diodes could reach up to 20 MHz. SINR measurements were conducted with a Keysight N5227A network analyzer, controlled by a laptop running Matlab code for measurement control.

Funding. Research Grants Council of the Hong Kong SAR (C1009-22GF, CityU 11204823); UK Engineering and Physical Sciences Research Council (EPSRC) (EP/W026813/1); Hong Kong Metropolitan University Staff Research Startup Fund (FRSF/2024/03); Shenzhen-Hong Kong-Macau Science and Technology Project (CategoryC) (SGDX20230821100459006).

Optics EXPRESS

Acknowledgments. K. T., K. W., and H. W. suggested the concept and supervised the project. B. L. originated the idea for this work, designed the meta-fluid antenna and rich-scattering generators, and planned the experiments. B. L. also conducted the numerical simulations, measurements, and data analysis. All authors contributed to writing, discussing, and reviewing the manuscript.

Disclosures. The authors declare no conflicts of interest.

Data availability. Data underlying the results presented in this paper are not publicly available at this time but may be obtained from the authors upon reasonable request. Correspondence and reasonable requests for data and materials should be addressed to B. L. (liubaiyang@sztu.edu.cn), K. T. (ktong@hkmu.edu.hk) or H. W. (hang.wong@cityu.edu.hk).

Supplemental document. See Supplement 1 for supporting content.

References

1. A. El Essaili, S. Thorson, A. Jude, *et al.*, "Holographic communication in 5g networks," Eric. Tech. Rev. **2022**(5), 2–11 (2022).
2. J. C. Zhang, G.-B. Wu, M. K. Chen, *et al.*, "A 6g meta-device for 3d varifocal," Sci. Adv. **9**(4), eadf8478 (2023).
3. G. P. Fettweis, "The tactile internet: Applications and challenges," IEEE Veh. Technol. Mag. **9**(1), 64–70 (2014).
4. M. Simsek, A. Aijaz, M. Dohler, *et al.*, "5g-enabled tactile internet," IEEE J. Select. Areas Commun. **34**(3), 460–473 (2016).
5. R. Jia, S. Kumar, T. C. Tan, *et al.*, "Valley-conserved topological integrated antenna for 100-gbps thz 6g wireless," Sci. Adv. **9**(44), eadi8500 (2023).
6. S. Dang, O. Amin, B. Shihada, *et al.*, "What should 6g be?" Nat. Electron. **3**(1), 20–29 (2020).
7. F. Tariq, M. R. Khandaker, K.-K. Wong, *et al.*, "A speculative study on 6g," IEEE Wireless Commun. **27**(4), 118–125 (2020).
8. X. You, Y. Huang, S. Liu, *et al.*, "Toward 6g tkμ extreme connectivity: Architecture, key technologies and experiments," IEEE Wireless Commun. **30**(3), 86–95 (2023).
9. B. Xiong, Y. Liu, Y. Xu, *et al.*, "Breaking the limitation of polarization multiplexing in optical metasurfaces with engineered noise," Science **379**(6629), 294–299 (2023).
10. N. Bozinovic, Y. Yue, Y. Ren, *et al.*, "Terabit-scale orbital angular momentum mode division multiplexing in fibers," Science **340**(6140), 1545–1548 (2013).
11. B. Liu, J. Wu, Q. Zhang, *et al.*, "High-speed wide-angle sensing and imaging by wideband metasurfaces with joint frequency, polarization, and spatial diversities," Laser Photonics Rev. **18**(9), 2400207 (2024).
12. B. Liu, Q. Zhang, and H. Wong, "Multifunctional reconfigurable intelligent surface for wideband beamforming and frequency-and-spatial-diverse microwave sensing," IEEE Trans. Antennas Propag. (2024).
13. D. Yang, Y. Yuan, Q. Wu, *et al.*, "High-gain oam antenna with low profile utilizing integrated reflective metasurface," Antennas Wirel. Propag. Lett. **23**(1), 294–298 (2024).
14. Y. Yuan, W. Zhou, M. Fan, *et al.*, "Deformable perfect vortex wave-front modulation based on geometric metasurface in microwave regime," Chinese J. Elect. **34**(1), 64–72 (2025).
15. Y. Yuan, K. Zhang, Q. Wu, *et al.*, "Reaching the efficiency limit of arbitrary polarization transformation with non-orthogonal metasurfaces," Nat. Commun. **15**(1), 6682 (2024).
16. D. A. Urquiza Villalonga, H. OdetAlla, M. J. Fernández-Getino García, *et al.*, "Spectral efficiency of precoded 5g-nr in single and multi-user scenarios under imperfect channel knowledge: A comprehensive guide for implementation," Electronics **11**(24), 4237 (2022).
17. Z. Wang, J. Zhang, H. Du, *et al.*, "Extremely large-scale mimo: Fundamentals, challenges, solutions, and future directions," IEEE Wireless Commun. (2023).
18. L. Dai, B. Wang, Y. Yuan, *et al.*, "Non-orthogonal multiple access for 5g: solutions, challenges, opportunities, and future research trends," IEEE Commun. Mag. **53**(9), 74–81 (2015).
19. Y. Mao, O. Dizdar, B. Clerckx, *et al.*, "Rate-splitting multiple access: Fundamentals, survey, and future research trends," IEEE Commun. Surv. Tutor **24**(4), 2073–2126 (2022).
20. Y. Chen, A. Bayesteh, Y. Wu, *et al.*, "Toward the standardization of non-orthogonal multiple access for next generation wireless networks," IEEE Commun. Mag. **56**(3), 19–27 (2018).
21. K. B. Letaief, W. Chen, Y. Shi, *et al.*, "The roadmap to 6g: Ai empowered wireless networks," IEEE Commun. Mag. **57**(8), 84–90 (2019).
22. C.-K. Wen, W.-T. Shih, and S. Jin, "Deep learning for massive mimo csi feedback," IEEE Wireless Commun. Lett. **7**(5), 748–751 (2018).
23. H. He, S. Jin, C.-K. Wen, *et al.*, "Model-driven deep learning for physical layer communications," IEEE Wireless Commun. **26**(5), 77–83 (2019).
24. K. K. Wong, A. Shojaeifard, K.-F. Tong, *et al.*, "Performance limits of fluid antenna systems," IEEE Commun. Lett. **24**(11), 2469–2472 (2020).
25. K.-K. Wong, A. Shojaeifard, K.-F. Tong, *et al.*, "Fluid antenna systems," IEEE Trans. Wireless Commun. **20**(3), 1950–1962 (2021).
26. W. K. New, K.-K. Wong, H. Xu, *et al.*, "A tutorial on fluid antenna system for 6g networks: Encompassing communication theory, optimization methods and hardware designs," IEEE Commun. Surv. Tutor (2024).

Optics EXPRESS

27. K.-K. Wong, D. Morales-Jimenez, K.-F. Tong, *et al.*, "Slow fluid antenna multiple access," IEEE Trans. Commun. **71**(5), 2831–2846 (2023).
28. K.-K. Wong and K.-F. Tong, "Fluid antenna multiple access," IEEE Trans. Wireless Commun. **21**(7), 4801–4815 (2022).
29. N. Waqar, K.-K. Wong, K.-F. Tong, *et al.*, "Deep learning enabled slow fluid antenna multiple access," IEEE Commun. Lett. **27**(3), 861–865 (2023).
30. N. Waqar, K.-K. Wong, C.-B. Chae, *et al.*, "Opportunistic fluid antenna multiple access via team-inspired reinforcement learning," IEEE Trans. Wireless Commun. **23**(9), 12068–12083 (2024).
31. C. Borda-Fortuny, L. Cai, K. F. Tong, *et al.*, "Low-cost 3d-printed coupling-fed frequency agile fluidic monopole antenna system," IEEE Access **7**, 95058–95064 (2019).
32. Y. Huang, L. Xing, C. Song, *et al.*, "Liquid antennas: Past, present and future," IEEE Open J. Antennas Propag. **2**, 473–487 (2021).
33. S. Dash, C. Psomas, and I. Krikidis, "Selection of metallic liquid in sub-6 ghz antenna design for 6g networks," Sci. Rep. **13**(1), 20551 (2023).
34. Y. Shen, B. Tang, S. Gao, *et al.*, "Design and implementation of mmwave surface wave enabled fluid antennas and experimental results for fluid antenna multiple access," arXiv (2024).
35. S. Song and R. D. Murch, "An efficient approach for optimizing frequency reconfigurable pixel antennas using genetic algorithms," IEEE Trans. Antennas Propag. **62**(2), 609–620 (2014).
36. J. Zhang, J. Rao, Z. Ming, *et al.*, "A pixel-based reconfigurable antenna design for fluid antenna systems," arXiv (2024).
37. H. L. Wang, H. F. Ma, Y. K. Zhang, *et al.*, "Multichannel highly secure wireless communication system with information camouflage capability," Sci. Adv. **10**(21), eadk7557 (2024).
38. L. Zhang, X. Q. Chen, S. Liu, *et al.*, "Space-time-coding digital metasurfaces," Nat. Commun. **9**(1), 4334 (2018).
39. V. Fusco, M. A. B. Abbasi, O. Yurduseven, *et al.*, "Single-pixel polarimetric direction of arrival estimation using programmable coding metasurface aperture," Nat. Sci. Rep. **11**(1), 23830 (2021).
40. L. Zhang, M. Z. Chen, W. Tang, *et al.*, "A wireless communication scheme based on space-and frequency-division multiplexing using digital metasurfaces," Nat. Electron. **4**(3), 218–227 (2021).
41. G.-B. Wu, J. Y. Dai, Q. Cheng, *et al.*, "Sideband-free space-time-coding metasurface antennas," Nat. Electron. **5**(11), 808–819 (2022).
42. S. R. Wang, J. Y. Dai, Q. Y. Zhou, *et al.*, "Manipulations of multi-frequency waves and signals via multi-partition asynchronous space-time-coding digital metasurface," Nat. Commun. **14**(1), 5377 (2023).
43. G.-B. Wu, J. Y. Dai, K. M. Shum, *et al.*, "A universal metasurface antenna to manipulate all fundamental characteristics of electromagnetic waves," Nat. Commun. **14**(1), 5155 (2023).
44. G.-B. Wu, J. Y. Dai, K. M. Shum, *et al.*, "A synthetic moving-envelope metasurface antenna for independent control of arbitrary harmonic orders," Nat. Commun. **15**(1), 7202 (2024).
45. N. J. Karl, R. W. McKinney, Y. Monnai, *et al.*, "Frequency-division multiplexing in the terahertz range using a leaky-wave antenna," Nat. Photonics **9**(11), 717–720 (2015).
46. M. Memarian and G. V. Eleftheriades, "Dirac leaky-wave antennas for continuous beam scanning from photonic crystals," Nat. Commun. **6**(1), 5855 (2015).
47. H. Matsumoto, I. Watanabe, A. Kasamatsu, *et al.*, "Integrated terahertz radar based on leaky-wave coherence tomography," Nat. Electron. **3**(2), 122–129 (2020).
48. G. Xu, A. Overvig, Y. Kasahara, *et al.*, "Arbitrary aperture synthesis with nonlocal leaky-wave metasurface antennas," Nat. Commun. **14**(1), 4380 (2023).
49. L. Zhu and K.-K. Wong, "Historical review of fluid antenna and movable antenna," arXiv (2024).
50. H. Yang, K.-K. Wong, K.-F. Tong, *et al.*, "Performance analysis of slow fluid antenna multiple access in noisy channels using gauss-laguerre and gauss-hermite quadratures," IEEE Commun. Lett. **27**(7), 1734–1738 (2023).
51. H. Xu, K.-K. Wong, W. K. New, *et al.*, "Revisiting outage probability analysis for two-user fluid antenna multiple access system," IEEE Transactions on Wireless Communications (2024).
52. Y. F. Wu, Y. Guo, and Y. J. Cheng, "Self-progressive near-field focusing 2-d full frequency scanning slot array antenna based on ridge-gap waveguide," IEEE Trans. Antennas Propag. **71**(1), 639–649 (2023).
53. G. L. Stüber and G. L. Steuber, *Principles of mobile communication*, vol. 2 (Springer, 2001).
54. H. Xu, G. Zhou, K.-K. Wong, *et al.*, "Channel estimation for fas-assisted multiuser mmwave systems," IEEE Commun. Lett. **28**(3), 632–636 (2024).
55. Z. Chai, K.-K. Wong, K.-F. Tong, *et al.*, "Port selection for fluid antenna systems," IEEE Commun. Lett. **26**(5), 1180–1184 (2022).
56. K.-K. Wong, C. Wang, H. Zhang, *et al.*, "Virtual fas by learning-based imaginary antennas," IEEE Wireless Commun. Letters (2024).
57. H. Zhang, J. Wang, C. Wang, *et al.*, "Learning-induced channel extrapolation for fluid antenna systems using asymmetric graph masked autoencoder," IEEE Wireless Commun. Lett. **13**(6), 1665–1669 (2024).
58. C. Wang, G. Li, H. Zhang, *et al.*, "Fluid antenna system liberating multiuser mimo for isac via deep reinforcement learning," IEEE Trans. Wireless Commun. **23**(9), 10879–10894 (2024).
59. M. Eskandari, A. G. Burr, K. Cumanan, *et al.*, "cgan-based slow fluid antenna multiple access," IEEE Wireless Commun. Lett. **13**(10), 2907–2911 (2024).
60. C. Wang, Z. Li, K.-K. Wong, *et al.*, "Ai-empowered fluid antenna systems: Opportunities, challenges, and future directions," IEEE Wireless Commun. **31**(5), 34–41 (2024).